

Cohort-Aware Agents for Individualized Lung Cancer Risk Prediction Using a Retrieval-Augmented Model Selection Framework

Chongyu Qu^a, Allen J. Luna^b, Thomas Z. Li^{a,b}, Junchao Zhu^a, Junlin Guo^a, Juming Xiong^a,
Kim L. Sandler^b, Bennett A. Landman^{a,b}, and Yuankai Huo^a

^aVanderbilt University, Nashville TN 37235, USA

^bVanderbilt University Medical Center, Nashville TN 37232, USA

ABSTRACT

Accurate lung cancer risk prediction remains challenging due to substantial variability across patient populations and clinical settings—**no single model performs best for all cohorts**. To address this, we propose personalized lung cancer risk prediction agent that dynamically selects the most appropriate model for each patient by combining cohort-specific knowledge with modern retrieval and reasoning techniques. Given a patient’s CT scan and structured metadata—including demographic, clinical, and nodule-level features—the agent **first** performs cohort retrieval using FAISS-based similarity search across nine diverse real-world cohorts to identify the most relevant patient population from a multi-institutional database. **Second**, a Large Language Model (LLM) is prompted with the retrieved cohort and its associated performance metrics to recommend the optimal prediction algorithm from a pool of eight representative models, including classical linear risk models (e.g., Mayo, Brock), temporally-aware models (e.g., TDVIT, DLSTM), and multi-modal computer vision based approaches (e.g., Liao, Sybil, DLS, DLI). This two-stage agent pipeline—retrieval via FAISS and reasoning via LLM—enables dynamic, cohort-aware risk prediction personalized to each patient’s profile. Building on this architecture, the agent supports flexible and cohort-driven model selection across diverse clinical populations, offering a practical path toward individualized risk assessment in real-world lung cancer screening.

Keywords: AI Agent, Retrieval-augmented Generation, Risk Prediction

1. INTRODUCTION

Accurate risk prediction for lung cancer remains a critical challenge in medical AI, particularly in large-scale screening^{1,2} programs and incidental nodule evaluation.^{2–6} Despite the wide variety of available predictive models—ranging from classical statistical risk scores^{7,8} to sophisticated computer vision based approaches^{9–12}—recent studies have consistently shown that no single model achieves optimal performance across all clinical contexts or patient populations.¹³ Cohort-specific characteristics, variability in imaging protocols,^{14–16} and differences in patient demographics routinely lead to substantial distribution shifts.^{17–19} Consequently, predictive models often experience large performance degradation when applied out-of-domain (OOD).^{20–28}

Retrieval-augmented modeling^{29,30} approaches have recently emerged as a promising paradigm to address such distributional challenges. By retrieving relevant contextual information from external knowledge bases or historical databases, these methods provide critical context to inform downstream reasoning tasks. In domains such as natural language processing, retrieval-augmented generation (RAG)³¹ techniques have demonstrated substantial improvements in task-specific accuracy and generalization.^{32,33} In clinical prediction, where understanding a patient’s specific cohort context can be decisive, retrieval strategies offer similar potential by leveraging patient-specific metadata and imaging features to identify clinically relevant reference cohorts, enabling more informed downstream model selection decisions.

Further author information: (Send correspondence to Yuankai Huo)

E-mail: yuankai.huo@vanderbilt.edu

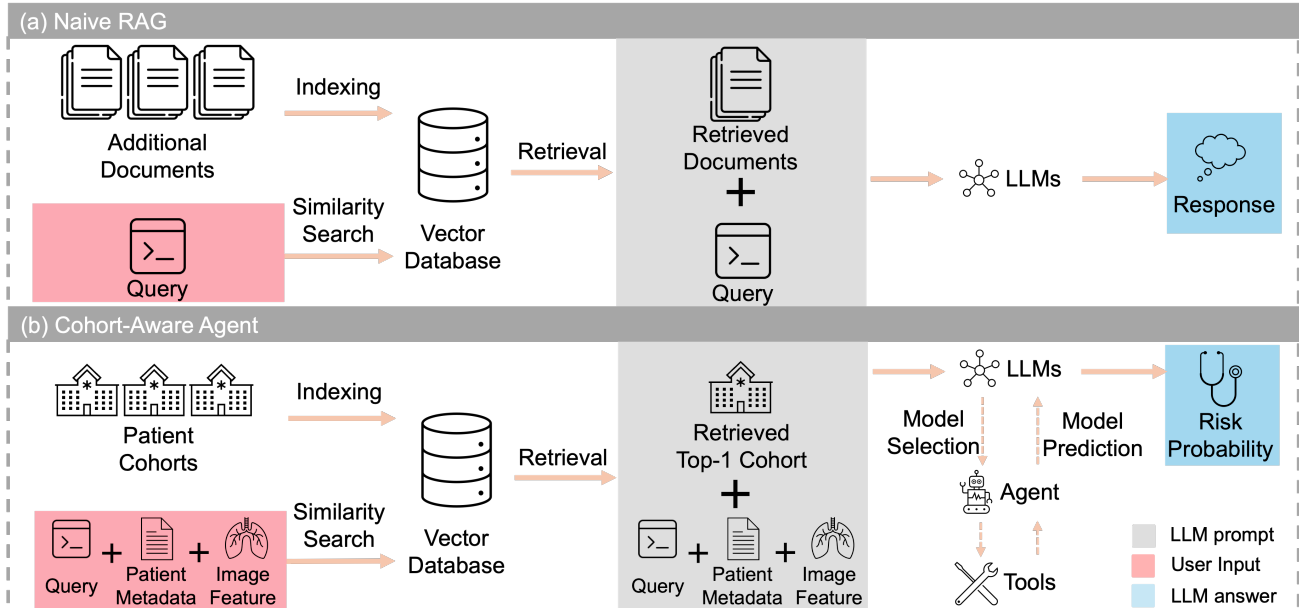


Figure 1: **Cohort-aware agent vs. naive RAG.** (a) Naive RAG retrieves context primarily based on a user query and applies a fixed reasoning process. In contrast, our (b) cohort-aware agent uses patient metadata and imaging features to retrieve the most relevant reference cohort. The agent then constructs an LLM prompt that includes the full patient profile, the retrieved cohort, and the prediction task. The LLM selects an appropriate model by invoking tools and returns a personalized lung cancer risk prediction.

However, to fully realize this potential, flexible reasoning systems that dynamically leverage retrieved context are necessary. Agent-based AI systems^{34–36} particularly those powered LLMs³⁷ have recently demonstrated remarkable flexibility in orchestrating multimodal reasoning³⁶ and decision making tasks.³⁸ Despite these advances, existing agent frameworks remain predominantly designed for general-purpose tasks. Their suitability for clinical prediction remains limited, especially in complex scenarios such as lung cancer risk assessment,^{39,40} where substantial variations across patient cohorts severely constrain the effectiveness of general-purpose reasoning strategies. In clinical contexts characterized by heterogeneous patient populations and substantial distribution shifts, relying on a single unified reasoning or predictive approach is inadequate. This highlights a key limitation of current agent-based frameworks: the absence of mechanisms to adapt decision-making to cohort-specific clinical contexts in a personalized and data-driven way.

To address this gap, we propose Cohort-Aware Agents, a retrieval-augmented framework for individualized lung cancer risk prediction. Rather than applying a fixed model across all patients, our approach automatically selects the most appropriate prediction algorithm by combining cohort retrieval with LLM-based reasoning. The agent follows a two-stage architecture inspired by clinical decision-making. In the **first** stage, it retrieves the most relevant reference cohort by comparing a patient’s CT scan and structured clinical metadata—including demographic,⁴¹ clinical, and nodule-level features—with a large, multi-institutional database using FAISS-based⁴² similarity search. This allows the agent to match each patient to a representative clinical subpopulation, capturing subtle patterns in data distribution. In the **second** stage, a LLM is prompted with the retrieved cohort’s characteristics and associated model performance summaries to identify the most suitable prediction algorithm. Rather than applying a fixed model, our agent dynamically selects from eight risk models, including classical statistical scores (e.g., Mayo,⁷ Brock⁸), temporally-aware models (e.g., TDVIT,⁹ DLSTM¹⁰), and computer vision based approaches (e.g., Liao,⁴³ Sybil,⁴⁴ DLS,¹² DLI¹¹). Figure 1 illustrates this overall framework by contrasting our cohort-aware agent with a naive RAG baseline. Our cohort-aware agent enables personalized, context-aware model selection that adapts to cohort-specific characteristics, providing a practical and generalizable solution for individualized lung cancer risk assessment. In summary, our agent makes the following contributions:

- *Cohort-aware patient retrieval:* We develop a FAISS-based retrieval strategy that identifies the most rel-

evant reference cohort for each patient by leveraging structured metadata and CT imaging features, enabling population-contextualized reasoning.

- *Retrieval-augmented model selection:* We design a two-stage agent pipeline where an LLM receives a patient’s profile and their most similar cohort retrieved from a FAISS-indexed database, and selects the optimal risk prediction model by referencing precomputed cohort-specific performance metrics.

- *Personalized risk prediction across diverse cohorts:* We demonstrate the effectiveness of our agent on nine real-world lung cancer screening cohorts and eight representative models, showing improved generalizability and individualized performance through cohort-driven model selection.

2. METHODS

Overview. We propose a Cohort-Aware Agent for individualized lung cancer risk prediction, built on a two-stage retrieval-augmented model selection framework, illustrate in Figure 2. Prior to inference, CT volumes from multiple cohorts are processed with the DeepLungScreening (DLS) pipeline to extract imaging features, which are concatenated with structured metadata and embedded into a FAISS-indexed vector database (Step 0). For a new patient, the same pipeline generates a query vector that is compared with the database to retrieve the top-1 cohort. During **cohort-aware patient retrieval** (§2.1, Step 1), this cohort provides population context for downstream reasoning. The patient’s metadata, CT-derived features, the top-1 cohort, and the task query together form the LLM prompt. During **retrieval-augmented model selection** (§2.2, Step 2), the LLM issues structured requests to the agent. The agent invokes tools to select the optimal model for that cohort, runs inference, and returns an individualized lung cancer risk probability. This design enables personalized, cohort-aware predictions and supports flexible, cohort-driven model selection across diverse clinical populations.

2.1 Cohort-aware patient retrieval

To provide population-contextualized reasoning, the agent first determines the most relevant reference cohort for each incoming patient. This step addresses the observation that predictive performance can vary markedly across patient populations due to distribution shifts in imaging protocols, demographic composition, and clinical characteristics. By retrieving a clinically similar cohort, the agent grounds its subsequent model selection in patterns that are specific to that population.

Each patient is represented by a multi-dimensional feature vector $\mathbf{x} \in \mathbb{R}^d$, defined as the concatenation of structured metadata (e.g., age, gender, smoking history) and imaging-derived features extracted from the CT scan. A similarity search module compares this patient vector against a pre-constructed vector database of prior cases, each associated with a known cohort label.

Let $\mathcal{D} = \{(\mathbf{x}_i, c_i)\}_{i=1}^N$ denote the indexed database, where $\mathbf{x}_i \in \mathbb{R}^d$ is the feature representation of the i -th patient, and $c_i \in \{1, \dots, C\}$ is the corresponding cohort label.

To identify similar cases, the agent performs approximate nearest-neighbor search over \mathcal{D} using FAISS. The top- k retrieved neighbors of \mathbf{x} are defined as:

$$\mathcal{N}_k(\mathbf{x}) = \text{TopK}_k(-\|\mathbf{x} - \mathbf{x}_i\|_2), \tag{1}$$

where $\|\cdot\|_2$ denotes the Euclidean (L2) norm. Cosine similarity may also be used depending on feature normalization.

The final retrieved cohort label \hat{c} is determined by majority vote over the cohort labels of the retrieved neighbors:

$$\hat{c} = \text{mode}(\{c_i \mid (\mathbf{x}_i, c_i) \in \mathcal{N}_k(\mathbf{x})\}). \tag{2}$$

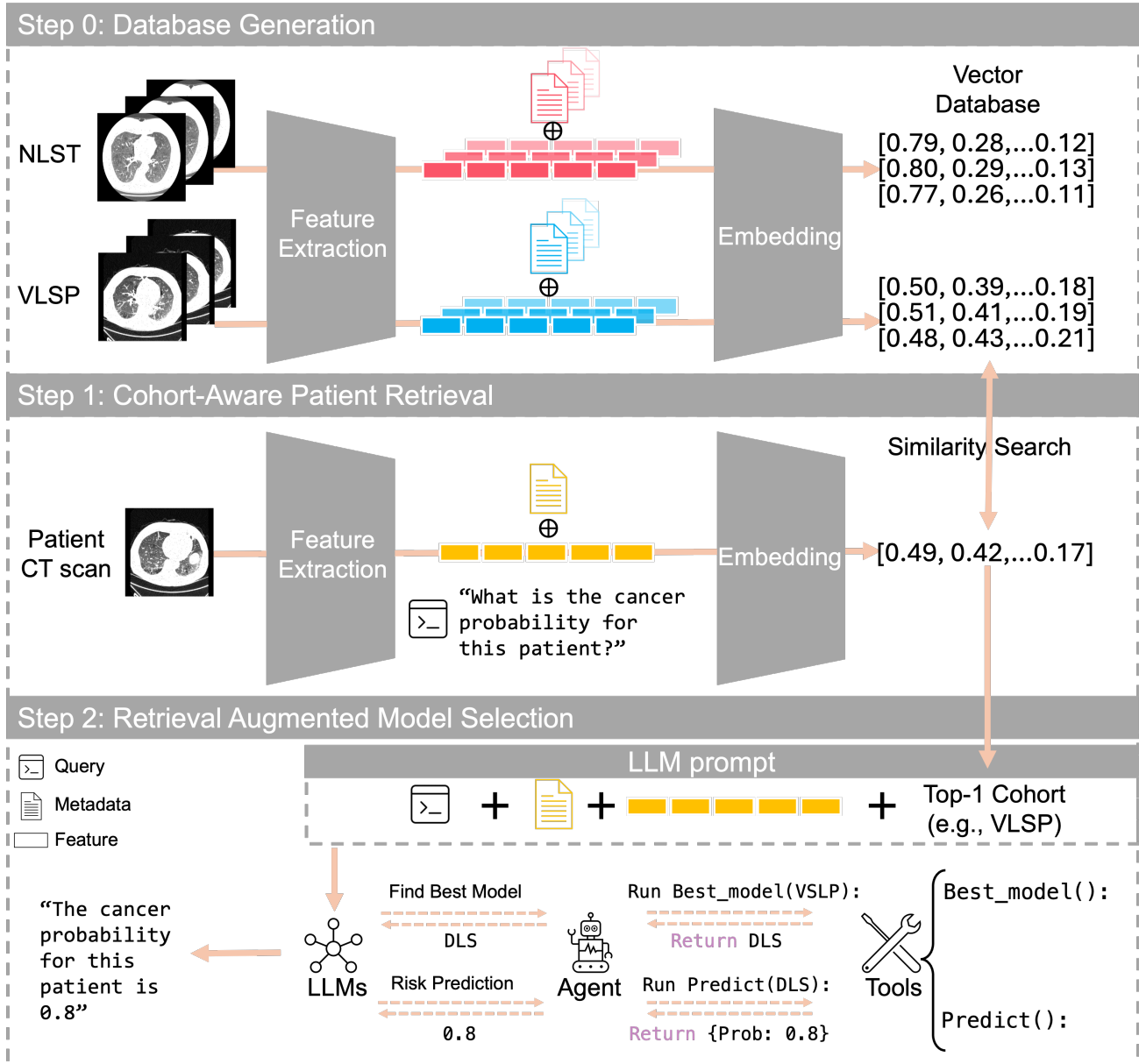


Figure 2: **The proposed Cohort-Aware Agents framework.** Patient metadata and imaging features are combined to retrieve the top-1 cohort. This cohort, together with the task query, guides the agent to select the optimal model via tool use and generate an individualized lung cancer risk prediction.

2.2 Retrieval-augmented model selection

Once the top-1 cohort \hat{c} has been identified, the agent proceeds to select the most appropriate lung cancer risk prediction model based on cohort context and patient-specific information. This stage leverages the reasoning capabilities of a LLM to coordinate model selection via tool use.

The LLM is prompted with the user-issued task query, the patient’s metadata and imaging-derived features (concatenated as \mathbf{x}), and the retrieved cohort \hat{c} . It returns a model selection decision as follows:

$$m^* = \text{LLM}(\text{query}, \mathbf{x}, \hat{c}), \quad (3)$$

where m^* denotes the identifier of the selected model. The agent then invokes this model and applies it to the

patient’s feature vector to generate a risk prediction:

$$\hat{y} = m^*(\mathbf{x}), \tag{4}$$

where \hat{y} is the predicted lung cancer risk probability. This completes the second stage of the framework, enabling cohort-adaptive, individualized inference.

3. DATA, MODEL AND EXPERIMENTAL SETTING

3.1 Cohort Overview

To ensure consistent image quality across cohorts, we applied a standardized set of preprocessing criteria. Specifically, we excluded CT scans with severe imaging artifacts, slice thickness ≥ 5 mm, or incomplete lung fields in the field of view.⁴⁵ All scans were de-identified using the MIRC Anonymizer⁴⁶ to remove protected health information. These quality and privacy controls help ensure comparability across institutions and enable robust representation learning from imaging data.

Our reference database comprises nine real-world lung cancer cohorts collected from diverse institutions and clinical contexts, each providing structured metadata, chest CT imaging, and diagnostic labels. The *VLSP* cohort comes from the Vanderbilt Lung Screening Program and represents a low-dose CT screening population. The *LIVUSPN*⁴⁷ cohort includes individuals enrolled in a longitudinal imaging and biomarker study, covering both high-risk and screening-detected cases. From the Multi-Center Lung (MCL) project, we incorporate four institution-specific cohorts: *MCL-VUMC* (Vanderbilt University Medical Center), *MCL-UPMC* (University of Pittsburgh Medical Center), *MCL-UCD* (University of California, Davis), and *MCL-DECAMP*⁴⁸ (from the DECAMP consortium), representing a mixture of screening, incidental, and diagnostic settings. The BRONCH cohort includes patients undergoing diagnostic bronchoscopy and is enriched for pathologically confirmed malignancies. We also include two subsets from the National Lung Screening Trial (NLST):⁴⁹ *NLST-test*,⁵⁰ a held-out split of the original trial, and *NLST-test-nodule*, a curated subset containing patients with confirmed pulmonary nodules.

All cohorts provide structured metadata suitable for similarity-based cohort retrieval, including features such as age, gender, BMI, smoking status, and scan date. In addition, each cohort includes nodule-level imaging features derived from chest CTs, along with binary cancer outcome labels confirmed through pathology or long-term follow-up. This consistency across cohorts enables robust construction of patient representations and supports cohort-aware retrieval and model selection within our framework.

3.2 Model Pool

Our agent selects from a pool of eight lung cancer risk prediction models, representing a diverse set of modeling paradigms and clinical assumptions. These models are grouped into three broad categories:

Linear risk models. The Mayo⁷ and Brock^{7,8} models are classical statistical scores based on logistic regression, widely used in clinical practice. They estimate malignancy risk using variables such as nodule size, patient age, smoking status, and spiculation. These models offer interpretability and strong baseline performance but are limited by their handcrafted feature^{51–53} sets and lack of imaging representation.

Temporally-aware models. TDVIT⁹ and DLSTM¹⁰ incorporate temporal information from sequential scans to model nodule evolution over time. TDVIT uses a transformer architecture with scan-position embeddings, while DLSTM leverages recurrent structures to track longitudinal changes. These models are applicable only to cohorts with multiple timepoints available.⁵⁴

Computer vision based models. Liao,⁴³ Sybil,⁴⁴ DeepLungScreening (DLS),¹² and DeepLungIPN (DLI)¹¹ utilize CT imaging, often in combination with structured metadata, to learn high-dimensional predictive features. Liao and Sybil focus on nodule- and whole-lung-based representations, respectively. DLS is optimized for screening populations, while DLI is designed for incidental and diagnostic settings and requires additional metadata fields.⁵⁵ Because of their differing input requirements, not all models are applied to all cohorts.

Model selection is performed adaptively by the agent based on availability of required inputs and historical performance on retrieved cohorts.

3.3 Implementation details.

We include 3,750 patients from nine cohorts, with per-cohort sizes ranging from 104 to 868. A random 30% of patients are held out for validation, while the remaining 70% form the retrieval database. During evaluation, each validation patient retrieves from this database for cohort-aware model selection. Patient representations are constructed by concatenating structured metadata (e.g., age, gender, BMI, smoking status) with pooled imaging features. The imaging features are extracted using the DLS pipeline, which produces a 5×128 feature map per case. This map is pooled and re-weighted by a factor of 0.1 before fusion with metadata. Similarity search is performed using FAISS with cosine distance, retrieving the top- $k = 15$ neighbors. Model selection is performed using TinyLlama-1.1B-Chat-v1.0 (FP16),⁵⁶ prompted with (i) the retrieved top-1 cohort, (ii) patient’s metadata and imaging-derived features, and (iii) user-issued task query. The LLM returns the name of the most suitable model, which is then used to produce the final risk prediction. The full agent pipeline—including retrieval, prompting, and inference—runs on a single NVIDIA A6000 GPU (48GB), without the need for distributed computation.

4. RESULTS

4.1 Cohort-Aware Retrieval Performance

To evaluate the retrieval component of our agent, we assess its ability to correctly identify the ground-truth cohort for each validation patient based on top-1 neighbor vote. As described in Section 2.2, all experiments use a fixed top- $k = 15$ for FAISS retrieval and apply a feature weight of 0.1 when combining metadata and imaging features.

The imaging features are extracted using the DLS pipeline, which outputs a 5×128 feature map per patient. We experiment with two aggregation strategies: flattening the feature map into a single 640-dimensional vector, or applying average pooling across the temporal axis to produce a 128-dimensional embedding. These representations are then concatenated with structured metadata to form the final retrieval vector. We also compare L2 and cosine similarity metrics.

Table 1: Top-1 accuracy of cohort retrieval under different input configurations and similarity metrics.

Input Type	Feature Aggregation	Similarity Metric	Top-1 Accuracy
Metadata only	—	L2	0.639
Metadata + Feature	Flattened	L2	0.222
Metadata + Feature	Pooled	L2	0.595
Metadata + Feature	Pooled	Cosine	0.667

The results are summarized in Table 1. Metadata alone provides a strong baseline with a top-1 accuracy of 0.639. Adding flattened imaging features significantly reduces accuracy to 0.222, likely due to high-dimensional noise and scale mismatches that negatively affect L2-based similarity. Aggregating the imaging features via average pooling improves stability and brings the accuracy back up to 0.595, though still slightly below the metadata-only baseline. The best performance is achieved when pooled imaging features are combined with cosine similarity, which normalizes vector magnitudes and better balances the influence of metadata and imaging inputs. This configuration yields a top-1 retrieval accuracy of 0.667, surpassing all other settings. These results highlight the importance of both appropriate feature aggregation and distance metric selection when integrating heterogeneous inputs for cohort retrieval.

To better understand retrieval behavior across different cohorts, we present a confusion matrix in Table 2, computed using the best-performing configuration (Metadata + Pooled Feature + Cosine). In this matrix, each row corresponds to the ground-truth cohort of a validation patient, while each column shows the top-1 cohort retrieved by the similarity searching. Diagonal entries indicate correct retrieval.

Perfect retrieval is observed for cohorts such as bronch and vlsp, which are highly distinct in both metadata and imaging space. In contrast, cohorts like mcl_upmc and nlst_test_nodule are more frequently misassigned, often confused with adjacent cohorts that share similar population characteristics. These patterns suggest that retrieval quality is influenced by inter-cohort similarity in the embedding space, which in turn affects downstream model selection accuracy.

Table 2: **Top-1 Cohort Retrieval Confusion Matrix.** Results are from the *Metadata + Pooled Feature + Cosine* configuration. Rows denote ground-truth cohorts, and columns show the retrieved top-1 cohorts. Diagonal entries correspond to correctly retrieved cases, with an overall accuracy of 0.667.

	branch	mcl_vumc	mcl_upmc	mcl_decamp	mcl_ucd	vlspl	livuspn	nlst_test_nodule	nlst_test	correct / total (acc)
branch	109	0	0	0	0	0	0	0	0	109 / 109 (1.000)
mcl_vumc	0	63	1	0	18	0	0	0	0	63 / 82 (0.768)
mcl_upmc	0	22	3	0	6	0	0	0	0	3 / 31 (0.097)
mcl_decamp	0	14	0	19	3	0	0	0	0	19 / 36 (0.528)
mcl_ucd	0	19	0	0	13	0	0	0	0	13 / 32 (0.406)
vlspl	0	0	0	0	0	256	0	0	1	256 / 257 (0.996)
livuspn	1	0	0	0	0	0	45	0	15	45 / 61 (0.738)
nlst_test_nodule	0	0	0	0	0	0	2	48	205	48 / 255 (0.188)
nlst_test	0	0	0	0	0	0	2	65	193	193 / 260 (0.742)
Overall										749 / 1123 (0.667)

4.2 Model Selection Performance

Table 3: **Cohort-wise AUC and Inference Time (s) under Different Model Selection Strategies.** The first three columns correspond to single-model baselines, Single Model (DLI, DLS, Sybil), where a fixed model is used across all cohorts. The **Per-Cohort Best Model** selects the best-performing model for each cohort based on pre-computed validation performance. The **Retrieval Model** reports the performance of our cohort-aware agent, which retrieves a top-1 similar cohort for each validation case and applies that cohort’s best-performing model

Cohort	Single Model (DLI)		Single Model (DLS)		Single Model (Sybil)		Per-Cohort Best Model		Retrieval Model	
	AUC	Time (s)	AUC	Time (s)	AUC	Time (s)	AUC	Time (s)	AUC	Time (s)
branch	0.609	0.55	0.643	0.55	0.657	1355.51	0.657	1296.04	0.660	1331.15
mcl_vumc	0.827	0.39	0.765	0.39	0.829	875.76	0.829	827.01	0.804	1064.71
mcl_upmc	0.983	0.33	0.880	0.33	0.923	199.02	0.983	0.50	1.000	0.30
mcl_decamp	0.738	0.34	0.753	0.34	0.654	365.96	0.753	0.35	0.761	0.32
mcl_ucd	0.938	0.33	0.805	0.34	0.801	349.33	0.938	0.34	0.892	0.46
vlspl	0.510	0.63	0.811	0.63	0.783	3325.91	0.811	0.67	0.810	0.62
livuspn	0.824	0.37	0.545	0.37	0.725	1011.29	0.824	0.38	0.842	0.36
nlst_test_nodule	0.545	0.61	0.627	0.61	0.853	1166.94	0.853	1173.90	0.982	498.98
nlst_test	0.534	0.64	0.634	0.64	0.838	1156.02	0.838	1197.63	0.840	2144.22
Overall	0.723	4.49	0.718	4.50	0.785	10805.84	0.832	4,496.82	0.843	5041.12

We evaluate the effectiveness of different model selection strategies in Table 3 and Figure 3 report the AUC, inference time and 97.5% confidence interval (CI) across cohorts under five configurations.

The first three strategies apply a *single model*—*DLI*, *DLS*, or *Sybil*—uniformly to all patients, regardless of cohort identity. Among these baselines, Sybil achieves the highest overall AUC (0.785), followed by DLI (0.723) and DLS (0.718). However, Sybil also incurs a substantially higher total inference time (10,805.84 seconds), reflecting the computational cost of its more complex architecture. In contrast, DLI and DLS are significantly more efficient, with total runtime under 5 seconds per cohort.

The Per-Cohort Best Model assigns to each cohort the model that historically achieved the best validation performance. This strategy relies on cohort identity and applies the corresponding best-performing model to all patients within that cohort. It improves the overall AUC to 0.832 while maintaining low total runtime (4,496.82 seconds), since a subset of cohort-optimal models are lightweight architectures such as DLI or DLS, though several cohorts still favor more complex models like Sybil. This result demonstrates the benefit of population-specific model allocation when accurate cohort information is available.

Our proposed *Retrieval Model* delivers performance comparable to the *Per-Cohort Best Model*. Across cohorts, the mean Δ AUC (Retrieval – Per-Cohort Best) is 0.0117 with a 95% bootstrap confidence interval [−0.0136, 0.0457] based on 1,000 resamples. For each validation case, the model retrieves the most similar cohort from the vector database via similarity search and then applies that cohort’s historically best model. This selection introduces minimal overhead and yields a competitive runtime (5041.12 seconds), comparable to the

Per-Cohort Best Model. These results support individualized, cohort-aware model selection in heterogeneous patient populations.

Figure 3 further summarizes the overall AUC and 97.5% confidence intervals under each strategy, confirming that the retrieval-based approach outperforms uniform and delivers performance comparable to cohort-specific baselines.

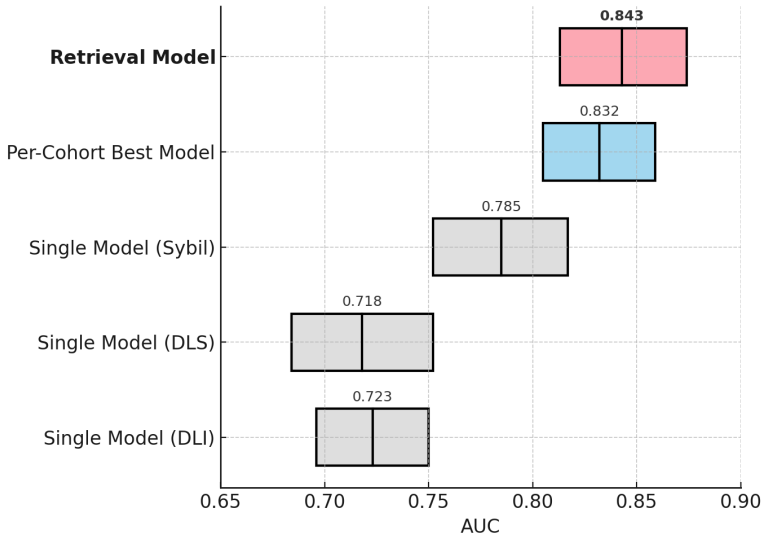


Figure 3: Overall AUC (Middle line) and 97.5 % CI (Box) under Different Model Selection Strategies.

5. CONCLUSION

We propose a cohort-aware agent for individualized lung cancer risk prediction, which leverages population-contextualized reasoning to select optimal predictive models for each patient. By retrieving clinically similar cohorts via a shared patient representation and applying a retrieval-based model selection strategy, our method accounts for distributional heterogeneity across institutions, imaging protocols, and demographics. Extensive evaluation across nine cohorts shows that our agent consistently achieves state-of-the-art performance, outperforming all single-model baselines and delivering results comparable to cohort-specific oracle assignments. This framework offers a scalable and adaptable solution for personalized risk prediction in real-world deployment settings, and illustrates the potential of retrieval-augmented agents to support data-driven generalization across diverse clinical populations.

ACKNOWLEDGMENTS

This research was supported by the National Institutes of Health (NIH) through grants F30CA275020, 2U01CA152662, R01CA253923 (Landman & Maldonado), R01CA275015 (Maldonado & Lenburg), U01CA152662 (Grogan), U01CA196405 (Maldonado), and P30CA068485-29S1, as well as the National Science Foundation (NSF) through CAREER 1452485 and grant 2040462. Additional support was provided by the Vanderbilt Institute for Surgery and Engineering through T32EB021937-07, the Vanderbilt Institute for Clinical and Translational Research via UL1TR002243-06, the Pierre Massion Directorship in Pulmonary Medicine, and the American College of Radiology Fund for Collaborative Research in Imaging (FCRI) Grant. This manuscript was polished using AI-assisted editing (ChatGPT) with a “rephrase” prompt; no scientific content was generated or altered.

REFERENCES

- [1] Rivera, M. P., Mehta, A. C., and Wahidi, M. M., “Establishing the diagnosis of lung cancer: Diagnosis and management of lung cancer: American college of chest physicians evidence-based clinical practice guidelines,” *Chest* **143**(5), e142S–e165S (2013).
- [2] Lokhandwala, T., Bittoni, M. A., Dann, R. A., D’Souza, A. O., Johnson, M., Nagy, R. J., Lanman, R. B., Merritt, R. E., and Carbone, D. P., “Costs of diagnostic assessment for lung cancer: a medicare claims analysis,” *Clinical lung cancer* **18**(1), e27–e34 (2017).
- [3] Gould, M. K., Tang, T., Liu, I.-L. A., Lee, J., Zheng, C., Danforth, K. N., Kosco, A. E., Di Fiore, J. L., and Suh, D. E., “Recent trends in the identification of incidental pulmonary nodules,” *American journal of respiratory and critical care medicine* **192**(10), 1208–1214 (2015).
- [4] Mazzone, P. J. and Lam, L., “Evaluating the patient with a pulmonary nodule: a review,” *Jama* **327**(3), 264–273 (2022).
- [5] MacMahon, H., Naidich, D. P., Goo, J. M., Lee, K. S., Leung, A. N., Mayo, J. R., Mehta, A. C., Ohno, Y., Powell, C. A., Prokop, M., et al., “Guidelines for management of incidental pulmonary nodules detected on ct images: from the fleischner society 2017,” *Radiology* **284**(1), 228–243 (2017).
- [6] Detterbeck, F. C., Lewis, S. Z., Diekemper, R., Addrizzo-Harris, D., and Alberts, W. M., “Executive summary: diagnosis and management of lung cancer: American college of chest physicians evidence-based clinical practice guidelines,” *Chest* **143**(5), 7S–37S (2013).
- [7] McWilliams, A., Tammemagi, M. C., Mayo, J. R., Roberts, H., Liu, G., Soghrati, K., Yasufuku, K., Martel, S., Laberge, F., Gingras, M., et al., “Probability of cancer in pulmonary nodules detected on first screening ct,” *New England journal of medicine* **369**(10), 910–919 (2013).
- [8] Swensen, S. J., Silverstein, M. D., Ilstrup, D. M., Schleck, C. D., and Edell, E. S., “The probability of malignancy in solitary pulmonary nodules: application to small radiologically indeterminate nodules,” *Archives of internal medicine* **157**(8), 849–855 (1997).
- [9] Li, T. Z., Xu, K., Gao, R., Tang, Y., Lasko, T. A., Maldonado, F., Sandler, K. L., and Landman, B. A., “Time-distance vision transformers in lung cancer diagnosis from longitudinal computed tomography,” in [*Medical Imaging 2023: Image Processing*], **12464**, 229–238, SPIE (2023).
- [10] Gao, R., Tang, Y., Xu, K., Huo, Y., Bao, S., Antic, S. L., Epstein, E. S., Deppen, S., Paulson, A. B., Sandler, K. L., et al., “Time-distanced gates in long short-term memory networks,” *Medical image analysis* **65**, 101785 (2020).
- [11] Gao, R., Tang, Y., Xu, K., Kammer, M. N., Antic, S. L., Deppen, S., Sandler, K. L., Massion, P. P., Huo, Y., and Landman, B. A., “Deep multi-path network integrating incomplete biomarker and chest ct data for evaluating lung cancer risk,” in [*Medical Imaging 2021: Image Processing*], **11596**, 387–393, SPIE (2021).
- [12] Gao, R., Tang, Y., Khan, M. S., Xu, K., Paulson, A. B., Sullivan, S., Huo, Y., Deppen, S., Massion, P. P., Sandler, K. L., et al., “Cancer risk estimation combining lung screening ct with clinical data elements,” *Radiology: Artificial Intelligence* **3**(6), e210032 (2021).
- [13] Li, T. Z., Xu, K., Krishnan, A., Gao, R., Kammer, M. N., Antic, S., Xiao, D., Knight, M., Martinez, Y., Paez, R., et al., “Performance of lung cancer prediction models for screening-detected, incidental, and biopsied pulmonary nodules,” *Radiology: Artificial Intelligence* **7**(2), e230506 (2025).
- [14] Li, Y., Lu, L., Xiao, M., Dercle, L., Huang, Y., Zhang, Z., Schwartz, L. H., Li, D., and Zhao, B., “Ct slice thickness and convolution kernel affect performance of a radiomic model for predicting egfr status in non-small cell lung cancer: a preliminary study,” *Scientific reports* **8**(1), 17913 (2018).
- [15] Choe, J., Lee, S. M., Do, K.-H., Lee, G., Lee, J.-G., Lee, S. M., and Seo, J. B., “Deep learning-based image conversion of ct reconstruction kernels improves radiomics reproducibility for pulmonary nodules or masses,” *Radiology* **292**(2), 365–373 (2019).
- [16] Qu, C., Zhang, T., Qiao, H., Tang, Y., Yuille, A. L., Zhou, Z., et al., “Abdomenatlas-8k: Annotating 8,000 ct volumes for multi-organ segmentation in three weeks,” *Advances in Neural Information Processing Systems* **36**, 36620–36636 (2023).
- [17] Ktena, I., Wiles, O., Albuquerque, I., Rebuffi, S.-A., Tanno, R., Roy, A. G., Azizi, S., Belgrave, D., Kohli, P., Cemgil, T., et al., “Generative models improve fairness of medical classifiers under distribution shifts,” *Nature Medicine* **30**(4), 1166–1173 (2024).

- [18] Li, W., Qu, C., Chen, X., Bassi, P. R., Shi, Y., Lai, Y., Yu, Q., Xue, H., Chen, Y., Lin, X., et al., “Abdomenatlas: A large-scale, detailed-annotated, & multi-center dataset for efficient transfer learning and open algorithmic benchmarking,” *Medical Image Analysis* **97**, 103285 (2024).
- [19] Kull, M., Silva Filho, T. M., and Flach, P., “Beyond sigmoids: How to obtain well-calibrated probabilities from binary classifiers with beta calibration,” (2017).
- [20] Lasko, T. A., Strobl, E. V., and Stead, W. W., “Why do probabilistic clinical models fail to transport between sites,” *NPJ Digital Medicine* **7**(1), 53 (2024).
- [21] Elsahar, H. and Gallé, M., “To annotate or not? predicting performance drop under domain shift,” in [*Proceedings of the 2019 Conference on Empirical Methods in Natural Language Processing and the 9th International Joint Conference on Natural Language Processing (EMNLP-IJCNLP)*], 2163–2173 (2019).
- [22] Zhu, J., Deng, R., Yao, T., Xiong, J., Qu, C., Guo, J., Lu, S., Yin, M., Wang, Y., Zhao, S., et al., “Asign: an anatomy-aware spatial imputation graphic network for 3d spatial transcriptomics,” in [*Proceedings of the Computer Vision and Pattern Recognition Conference*], 30829–30838 (2025).
- [23] Zhu, J., Deng, R., Yao, T., Xiong, J., Qu, C., Guo, J., Lu, S., Tang, Y., Xu, D., Yin, M., et al., “Magnet: Multi-level attention graph network for predicting high-resolution spatial transcriptomics,” *arXiv preprint arXiv:2502.21011* (2025).
- [24] Zhu, J., Yin, M., Deng, R., Long, Y., Wang, Y., Wang, Y., Zhao, S., Yang, H., and Huo, Y., “Cross-species data integration for enhanced layer segmentation in kidney pathology,” in [*Medical Imaging 2025: Digital and Computational Pathology*], **13413**, 49–56, SPIE (2025).
- [25] Zhu, J., Shen, Y., Zhang, H., and Ke, J., “An anti-biased tbsrtc-category aware nuclei segmentation framework with a multi-label thyroid cytology benchmark,” in [*International Conference on Medical Image Computing and Computer-Assisted Intervention*], 580–590, Springer (2023).
- [26] Youssef, A., Pencina, M., Thakur, A., Zhu, T., Clifton, D., and Shah, N. H., “External validation of ai models in health should be replaced with recurring local validation,” *Nature Medicine* **29**(11), 2686–2687 (2023).
- [27] Hu, F., Chen, A. A., Horng, H., Bashyam, V., Davatzikos, C., Alexander-Bloch, A., Li, M., Shou, H., Satterthwaite, T. D., Yu, M., et al., “Image harmonization: A review of statistical and deep learning methods for removing batch effects and evaluation metrics for effective harmonization,” *NeuroImage* **274**, 120125 (2023).
- [28] Li, T.-W. and Lee, G.-C., “Performance analysis of fine-tune transferred deep learning,” in [*2021 IEEE 3rd Eurasia Conference on IOT, Communication and Engineering (ECICE)*], 315–319, IEEE (2021).
- [29] Blattmann, A., Rombach, R., Oktay, K., Müller, J., and Ommer, B., “Retrieval-augmented diffusion models,” *Advances in Neural Information Processing Systems* **35**, 15309–15324 (2022).
- [30] Gao, Y., Xiong, Y., Gao, X., Jia, K., Pan, J., Bi, Y., Dai, Y., Sun, J., Wang, H., and Wang, H., “Retrieval-augmented generation for large language models: A survey,” *arXiv preprint arXiv:2312.10997* **2**(1) (2023).
- [31] Lewis, P., Perez, E., Piktus, A., Petroni, F., Karpukhin, V., Goyal, N., Küttler, H., Lewis, M., Yih, W.-t., Rocktäschel, T., et al., “Retrieval-augmented generation for knowledge-intensive nlp tasks,” *Advances in neural information processing systems* **33**, 9459–9474 (2020).
- [32] Liu, H., Son, K., Yang, J., Liu, C., Gao, J., Lee, Y. J., and Li, C., “Learning customized visual models with retrieval-augmented knowledge,” in [*Proceedings of the IEEE/CVF Conference on Computer Vision and Pattern Recognition*], 15148–15158 (2023).
- [33] Zakka, C., Shad, R., Chaurasia, A., Dalal, A. R., Kim, J. L., Moor, M., Fong, R., Phillips, C., Alexander, K., Ashley, E., et al., “Almanac—retrieval-augmented language models for clinical medicine,” *Nejm ai* **1**(2), AIoa2300068 (2024).
- [34] Durante, Z., Huang, Q., Wake, N., Gong, R., Park, J. S., Sarkar, B., Taori, R., Noda, Y., Terzopoulos, D., Choi, Y., et al., “Agent ai: Surveying the horizons of multimodal interaction,” *arXiv preprint arXiv:2401.03568* (2024).
- [35] Huang, W., Abbeel, P., Pathak, D., and Mordatch, I., “Language models as zero-shot planners: Extracting actionable knowledge for embodied agents,” in [*International conference on machine learning*], 9118–9147, PMLR (2022).

- [36] Peng, B., Galley, M., He, P., Cheng, H., Xie, Y., Hu, Y., Huang, Q., Liden, L., Yu, Z., Chen, W., et al., “Check your facts and try again: Improving large language models with external knowledge and automated feedback,” *arXiv preprint arXiv:2302.12813* (2023).
- [37] Bubeck, S., Chandrasekaran, V., Eldan, R., Gehrke, J., Horvitz, E., Kamar, E., Lee, P., Lee, Y. T., Li, Y., Lundberg, S., et al., “Sparks of artificial general intelligence: Early experiments with gpt-4,” *arXiv preprint arXiv:2303.12712* (2023).
- [38] Gong, R., Huang, Q., Ma, X., Vo, H., Durante, Z., Noda, Y., Zheng, Z., Zhu, S.-C., Terzopoulos, D., Fei-Fei, L., et al., “Mindagent: Emergent gaming interaction,” *arXiv preprint arXiv:2309.09971* (2023).
- [39] Petit, P., Maitre, A., Persoons, R., and Bicout, D. J., “Lung cancer risk assessment for workers exposed to polycyclic aromatic hydrocarbons in various industries,” *Environment International* **124**, 109–120 (2019).
- [40] Guida, F., Sun, N., Bantis, L. E., Muller, D. C., Li, P., Taguchi, A., Dhillon, D., Kundnani, D. L., Patel, N. J., Yan, Q., et al., “Assessment of lung cancer risk on the basis of a biomarker panel of circulating proteins,” *JAMA oncology* **4**(10), e182078–e182078 (2018).
- [41] Tammemägi, M. C., Katki, H. A., Hocking, W. G., Church, T. R., Caporaso, N., Kvale, P. A., Chaturvedi, A. K., Silvestri, G. A., Riley, T. L., Commins, J., et al., “Selection criteria for lung-cancer screening,” *New England Journal of Medicine* **368**(8), 728–736 (2013).
- [42] Douze, M., Guzhva, A., Deng, C., Johnson, J., Szilvasy, G., Mazaré, P.-E., Lomeli, M., Hosseini, L., and Jégou, H., “The faiss library,” *arXiv preprint arXiv:2401.08281* (2024).
- [43] Liao, F., Liang, M., Li, Z., Hu, X., and Song, S., “Evaluate the malignancy of pulmonary nodules using the 3-d deep leaky noisy-or network,” *IEEE transactions on neural networks and learning systems* **30**(11), 3484–3495 (2019).
- [44] Mikhael, P. G., Wohlwend, J., Yala, A., Karstens, L., Xiang, J., Takigami, A. K., Bourgouin, P. P., Chan, P., Mrah, S., Amayri, W., et al., “Sybil: a validated deep learning model to predict future lung cancer risk from a single low-dose chest computed tomography,” *Journal of Clinical Oncology* **41**(12), 2191–2200 (2023).
- [45] Gao, R., Khan, M. S., Tang, Y., Xu, K., Deppen, S., Huo, Y., Sandler, K. L., Massion, P. P., and Landman, B. A., “Technical report: quality assessment tool for machine learning with clinical ct,” *arXiv preprint arXiv:2107.12842* (2021).
- [46] Radiological Society of North America (RSNA), “The mirc dicom anonymizer.” https://mircwiki.rsna.org/index.php?title=The_MIRC_DICOM_Anonymizer. MIRC Wiki. Accessed: 2025-08-19.
- [47] Li, T. Z., Xu, K., Chada, N. C., Chen, H., Knight, M., Antic, S., Sandler, K. L., Maldonado, F., Landman, B. A., and Lasko, T. A., “Curating retrospective multimodal and longitudinal data for community cohorts at risk for lung cancer,” *Cancer Biomarkers* **42**(1), CBM-230340 (2025).
- [48] Billatos, E., Duan, F., Moses, E., Marques, H., Mahon, I., Dymond, L., Apgar, C., Aberle, D., Washko, G., Spira, A., et al., “Detection of early lung cancer among military personnel (decamp) consortium: study protocols,” *BMC Pulmonary Medicine* **19**(1), 59 (2019).
- [49] Team, N. L. S. T. R., “Reduced lung-cancer mortality with low-dose computed tomographic screening,” *New England Journal of Medicine* **365**(5), 395–409 (2011).
- [50] Ardila, D., Kiraly, A. P., Bharadwaj, S., Choi, B., Reicher, J. J., Peng, L., Tse, D., Etemadi, M., Ye, W., Corrado, G., et al., “End-to-end lung cancer screening with three-dimensional deep learning on low-dose chest computed tomography,” *Nature medicine* **25**(6), 954–961 (2019).
- [51] Revel, M.-P., Bissery, A., Bienvenu, M., Aycard, L., Lefort, C., and Frija, G., “Are two-dimensional ct measurements of small noncalcified pulmonary nodules reliable?,” *Radiology* **231**(2), 453–458 (2004).
- [52] Oxnard, G. R., Zhao, B., Sima, C. S., Ginsberg, M. S., James, L. P., Lefkowitz, R. A., Guo, P., Kris, M. G., Schwartz, L. H., and Riely, G. J., “Variability of lung tumor measurements on repeat computed tomography scans taken within 15 minutes,” *Journal of Clinical Oncology* **29**(23), 3114–3119 (2011).
- [53] Devaraj, A., van Ginneken, B., Nair, A., and Baldwin, D., “Use of volumetry for lung nodule management: theory and practice,” *Radiology* **284**(3), 630–644 (2017).
- [54] Rudin, C. M., Brambilla, E., Faivre-Finn, C., and Sage, J., “Small-cell lung cancer,” *Nature Reviews Disease Primers* **7**(1), 3 (2021).

- [55] Kammer, M. N., Kussrow, A. K., Webster, R. L., Chen, H., Hoeksema, M., Christenson, R., Massion, P. P., and Bornhop, D. J., “Compensated interferometry measures of cyfra 21–1 improve diagnosis of lung cancer,” *ACS combinatorial science* **21**(6), 465–472 (2019).
- [56] Zhang, P., Zeng, G., Wang, T., and Lu, W., “Tynyllama: An open-source small language model,” *arXiv preprint arXiv:2401.02385* (2024).